Cosmetics **2015**, *2*, 1-x manuscripts; doi:10.3390/cosmetics20x000x

OPEN ACCESS

cosmetics

ISSN 2079-9284

www.mdpi.com/journal/cosmetics

Article

Photothermal Radiometry for Skin Research

Perry Xiao *

School of Engineering, London South Bank University, 103 Borough Road, London SE1 0AA, UK

* Author to whom correspondence should be addressed; E-Mail: xiaop@lsbu.ac.uk; Tel.: +44-207-815-7569; Fax: +44-207-815-7699.

Academic Editor:

Received: / Accepted: / Published:

Abstract: Photothermal radiometry is an infrared remote sensing technique that has been used for skin and skin appendages research, in the areas of skin hydration, hydration gradient, skin hydration depth profiling, skin thickness measurements, skin pigmentation measurements, effect of topically applied substances and transdermal drug delivery, moisture content of bio-materials, membrane permeation, nail and hair measurements. Comparing with other technologies, Photothermal radiometry has the advantages of non-contact, non-destructive, quick to make a measurement (a few seconds), and spectroscopic in nature. It also is colour blind, and can work on any arbitrary sample surfaces. It has a unique depth profiling capability on the sample surface (typically top 20 μm), which make it particularly suitable for skin measurements. In this paper, we present a review of the photothermal radiometry work carried out in our research group. We will first introduce the theoretical background, then illustrate its applications with experimental results.

Keywords: Photothermal radiometry; skin hydration; skin hydration depth profiling; trans-dermal drug delivery; hair and nail.

---

1. Introduction

Photothermal radiometry (PTR), or opto-thermal radiometry (OTR), is an infrared remote sensing technique that was independently developed by Tam et al [1] and Imhof et al [2] back in the 1980s. It has since been used for biomedical applications [3-5] and industrial non-destructive testing (NDT) [6,7]. Photothermal radiometry uses a modulated (sinusoidal or pulsed) light source (i.e. laser etc.) to

heat up the sample surface, and uses a fast infrared detector (e.g. mercury cadmium telluride or MCT) to pick up the sample's corresponding blackbody radiation due to the temperature increase. By analyzing the shape of the signal, we can get information on sample's optical properties, thermal properties, the thickness of the sample and its layer structure. The pulsed laser version – Opto-Thermal Transient Emission Radiometry (OTTER) - developed initially by Imhof et al [2,8,9] and consequently by Xiao et al [9-19], has been intensively used for skin and skin appendages measurements.

2. Theoretical Background

When an incident light beam reaches the skin surface, a small fraction of the light will be reflected due to the change in refractive index between air (n_{air}=1.0) and stratum corneum (n_{sc}=1.55). The rest of the light will pass through the surface and go into the skin, undergoing a process of multiple scattering and absorption [20]. Absorbed light energy is converted to heat which increases the temperature of the skin. Scattered light contributes to a diffuse distribution of light within the skin. Scattering and absorption determine the light penetration depth and light distribution within the skin. The degree of scattering and absorption depends on the wavelength of the incident light and the optical properties of the skin, which can be described by its absorption coefficient, its scattering coefficient and the anisotropy.

Some of the light travelling in the skin will also be reflected at the interfaces of the skin layers and blood vessels. Some of this reflected and back scattered light can travel through the skin and finally go back into the air. This is called the remitted light. The remittance from epidermis and dermis, together with the regular reflectance from the skin surface form the total remittance of the incident radiation, which give the colour of the skin. The measurement of this remittance can give information on erythema, blanching, melanin, glucose level, oxygen level, haemoglobin, blood flow and skin structure.

This light - tissue interactions can normally be divided into three domains: absorption domain, scattering domain and equal scattering and absorption domain. Absorption domain is where absorption events occur more rapidly than effective scattering events. This is true for some UV (193, 248, 308nm of ArK, KrF, XeCl excimer lasers) and the IR (2.94μm Er: YAG, 10.6μm CO2 lasers) wavelengths, where tissue absorption can be substantially larger than scattering. Scattering domain is where multiple scattering events occur before an absorption event occurs. This is true for the wavelengths between 600 and 1300 nm, where haemoglobin and melanin pigments do not absorb strongly [21]. The band between 600 and 1300 nm is often called “therapeutic window” which offers the possibility of treating large volumes with certain long-wavelength photosensitizers. Equal scattering and absorption domain is where both absorption and scattering are substantial, and light in the skin has a strongly collimated component surrounded by a region where light is multiply scattered. This is true for wavelengths between 450 and 590nm, which include the argon laser and Nd:YAG laser wavelengths, the penetration depth is approximately 0.5 to 2.5 mm [22].

OTTER technology mainly works in the absorption domain when 2.94μm Er:YAG laser is used and in the equal scattering and absorption domain when Nd:YAG laser (532nm) or OPO laser (420 – 590nm) is used. OTTER is only sensitive to absorbed light, due to the MCT infrared detector used. The reflected light, scattered light, and remitted light make no contribution to the OTTER signal.

After the laser pulse, the absorbed laser light energy will decay exponentially into deeper skin according to Beer-Lambert law, and the corresponding temperature changes inside skin can be described as,

$$\theta(z,0) = \frac{E_0 \alpha}{\rho C} e^{-\alpha z} \tag{1}$$

where $\theta(z,0)$ is the temperature at time t=0 of the skin at position z, with z=0 at the surface and increasing toward the inside of the skin. α is the absorbance for the excitation laser, C the specific heat, ρ the density, and E_0 the energy density absorbed from the excitation laser. This initial temperature will then re-distribute follows the diffusion law which, in general, can be expressed as

$$\begin{cases} \left(\frac{\partial}{\partial z} \left[D \times \frac{\partial}{\partial z} \right] - \frac{\partial}{\partial t} \right) \theta(z,t) = 0 \\ Initial \quad Condition: \quad \theta(z,t)\big|_{t=0} = \theta(z,0) \\ Boundary \quad Condition: -k \frac{\partial \theta(z,t)}{\partial z}\Big|_{z=0} = 0 \end{cases} \tag{2}$$

where D is the thermal diffusivity of the skin, and k is thermal conductivity of the skin. In skin measurements, we are mainly interested in optical properties, as thermal properties do not change very much. Therefore it is safe to assume the skin is thermally homogeneous, then Eq. (2) can be solved by using Green's function method, to yield a time-dependent transient temperature field as [10]

$$\theta(z,t) = \frac{E_0 \alpha}{2C\rho} e^{\alpha^2 Dt} \left\{ e^{-\alpha z} erfc\left(\frac{\alpha^2 Dt - \frac{1}{2}\alpha z}{\sqrt{\alpha^2 Dt}} \right) + e^{\alpha z} erfc\left(\frac{\alpha^2 Dt + \frac{1}{2}\alpha z}{\sqrt{\alpha^2 Dt}} \right) \right\} \tag{3}$$

where $erfc(x) = 1 - erf(x)$ is the complementary error function, $erf(x) = \frac{2}{\sqrt{\pi}} \int_0^x e^{-y^2} dy$ is error function.

The corresponding OTTER signal generated by this transient temperature $\theta(z,t)$ can be calculated by

$$S(t) = \frac{\zeta E_0 \beta}{\rho C} \int_0^\infty e^{-\beta z} \theta(z,t) dz \tag{4}$$

where β is the skin's absorption coefficient for the emitted thermal radiation, and the parameter $\zeta = \zeta(\lambda_{em})$ includes factors that depend on the black body emission curve, detector sensitivity, focusing and alignment, but is independent of the properties of the sample per se [2,8-10].

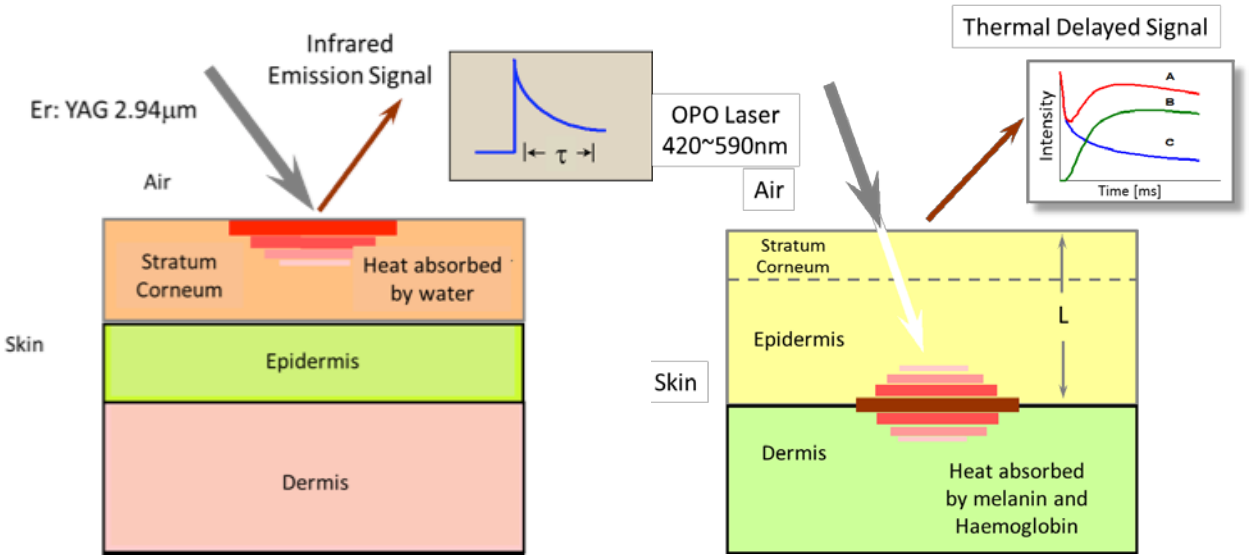

Figure 1. The schematic diagram for OTTER hydration measurements (left) and skin pigments measurements (right).

Figure 1 shows the schematic diagram for OTTER measurements. When Nd:YAG laser (532nm, 10ns pulse width) or OPO laser (420 – 590nm, 10ns pulse width) is used as the excitation heat source, see Figure 1 (right), the laser is mainly absorbed by melanin and haemoglobin deep inside the skin. In this case, we are measuring the skin pigments and epidermis thickness [10-14]. OTTER signal is typically a delayed thermal wave signal, and Eq.(4) can be solved and expressed as

$$S(t) = A_1 e^{t/\tau_1} erfc\sqrt{t/\tau_1} + A_2 \frac{e^{-\tau_2/t}}{\sqrt{t/\tau_2}} \quad (5)$$

where A_1 and A_2 are the signal amplitudes, $\tau_1 = 1/\alpha^2 D$ and $\tau_2 = L^2/4D$. Using Eq.(5) to fit the signal we can get the melanin and haemoglobin absorption (α) and epidermis thickness (L).

When the Er:YAG laser (2.94 μm wavelength, 100ns pulse width, a few mille joules per pulse) is used as the heat source, see Figure 1 (left), the laser is absorbed at the skin surface, by the water in the skin, and the measurements are confined within stratum corneum, the outmost skin layer (~ 20 μm in thickness). In this case, OTTER signal is typically a decay signal, and depending on the detection wavelength, the OTTER signals can either reflect the water concentration information in skin (13.1μm), or solvent concentration information within skin (9.5μm). By applying different mathematical models, we can get the average water content in stratum corneum [10], the water concentration gradient in stratum corneum [10, 15], and water concentration depth profiles or solvent concentration depth profiles in stratum corneum [16].

Homogeneous Model

If we assume the skin is optically homogeneous, and under the excitation saturation condition, i.e. $\alpha >> \beta$, (this is true when Er:YAG laser is used), then Eq.(4) can be solved and expressed as [1,8,9,10]

$$S(t) = Ae^{t/\tau} erfc\sqrt{t/\tau} \tag{6}$$

where A is the amplitude of the signal, $\tau = 1/\beta^2 D$ is the signal decay lifetime. By fitting Eq.(6) to OTTER signals we can the best-fit value for τ, which can then be related to average water or solvent concentration in the skin, depending on the detection wavelengths used.

Gradient Model

If we assume the skin is optically non-homogeneous, but has a linear gradient distribution, e.g.

$$\beta(z) = \beta_0 + wz \tag{7}$$

where β_0 is the absorption coefficient of the surface of the skin, and w is the gradient of the absorption coefficient. Then Eq.(4) can be solved and expressed as [10, 15]

$$S(t) = A \times \left(\frac{2W\sqrt{t\tau}}{\sqrt{\pi}(2Wt+1)} + \frac{1}{\sqrt{(2Wt+1)^3}} e^{\frac{t/\tau}{2t/\tau+1}} erfc\left(\frac{\sqrt{t/\tau}}{\sqrt{2Wt+1}}\right) \right) \tag{8}$$

Where $W = wD$ is the effective gradient and $\tau = 1/\beta_0^2 D$ is the signal decay lifetime. By fitting Eq.(8) to OTTER signals we can get information on τ and W, which can then be related to the skin surface water (or solvent) concentration, and the water (or solvent) concentration gradient within the skin [10,15].

Non-homogeneous Model

If we assume the skin is optically irregularly non-homogeneous, then Eq.(4) will be difficult to solve. But we can resolve this non-homogeneous issue using our Segmented Least-Squares (SLS) fitting technique [16]. Our previous study shows that for an OTTER decay signal, at different times after the laser excitation, on average, the signal comes from different depths, which we call it the "mean detection depth", $\bar{Z}(t)$. It can be calculated as [9]

$$\bar{Z}(t) = \frac{\int_0^\infty \beta e^{-\beta z} \cdot z \cdot \theta(z,t) dz}{\int_0^\infty \beta e^{-\beta z} \theta(z,t) dz} \tag{9}$$

where $\theta(z,t)$ is the transient temperature field. Again, under the excitation saturation condition ($\alpha >> \beta$), we have

$$\bar{Z}(t) = \frac{2}{\sqrt{\pi}} \times \frac{\sqrt{t/\tau}}{\beta e^{t/\tau} erfc\sqrt{t/\tau}} - 2 \times \frac{t/\tau}{\beta} \tag{10}$$

where $\overline{\beta}$ is the average value of β, calculated by using Eq.(6) to fit the whole time-span of the signal. Figure 2 shows a typical relationship between the OTTER signal S(t) and its corresponding mean detection depth $\overline{Z}(t)$ for a semi-infinite homogenous sample. So, in the case of surface dominant absorption, the initial signal data points give information about the surface of the sample, and later signal data points give information about deeper parts of the sample. In other cases, it depends on the sample's actual transient temperature $\theta(z,t)$ and emission absorption coefficient β .

Our Segmented Least-Squares (SLS) fitting data analysis technique is based on above principles [16]. First, we divide the signal data points into a series of small pieces. Second, we use a least-squares fitting routine to fit each piece separately to Eq.(6), to get the best-fit value of the decay lifetime τ for that piece. Finally, we relate each piece's τ to its mean radiation depth using Eq.(10), to create a depth-resolved τ profiles, which can then be related to the water (or solvent) concentration depth profiles within skin.

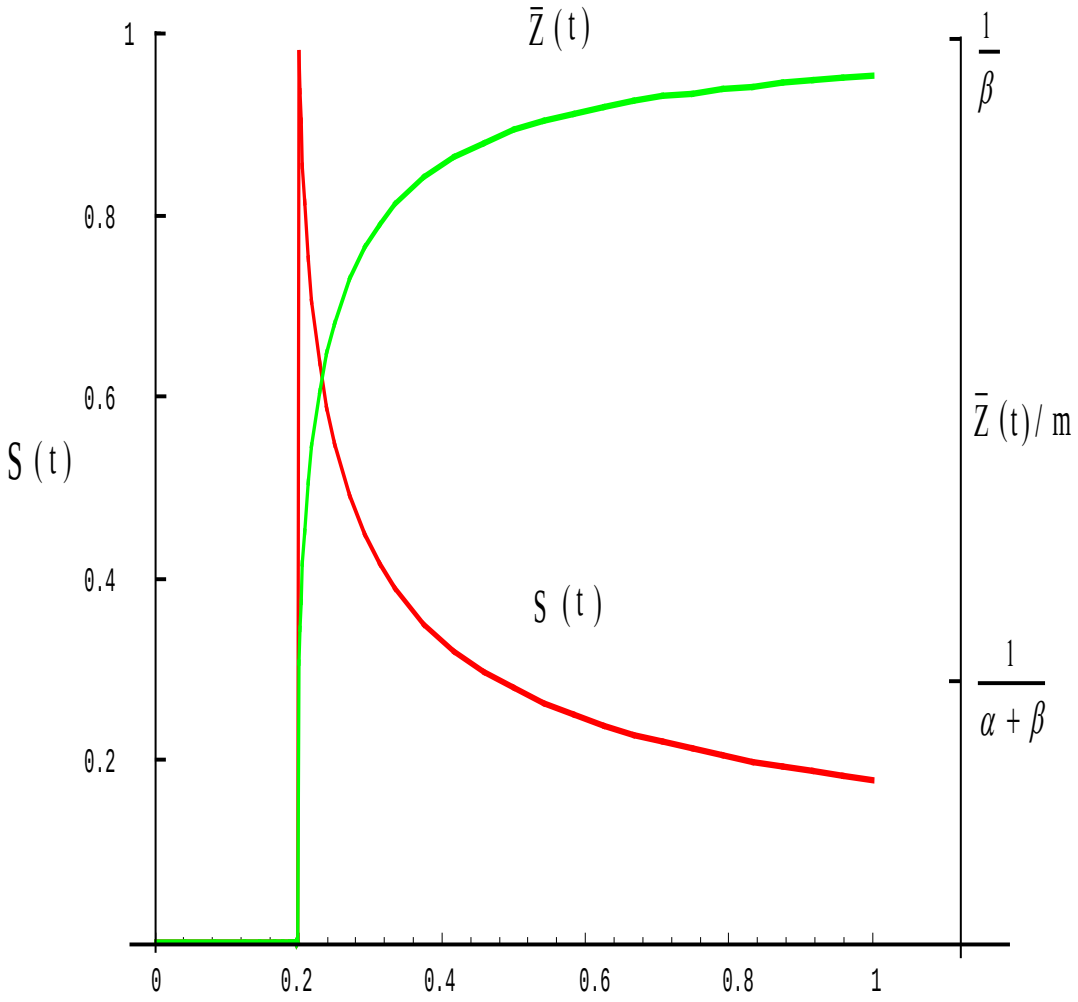

Figure 2. The OTTER signal and its average radiation depth [10].

3. OTTER Applications

3.1. Skin Pigment Measurements

In this case, Nd:YAG laser (532nm) or OPO laser (420 – 590nm) is used as the heat source in the measurements, and measurement signal is typically a delayed thermal wave. Figure 3 shows the typical signals of skin pigment measurements [10]. The hump in the signal, immediately after the initial decay, is due to the heat diffusion from deep inside the skin to skin surface.

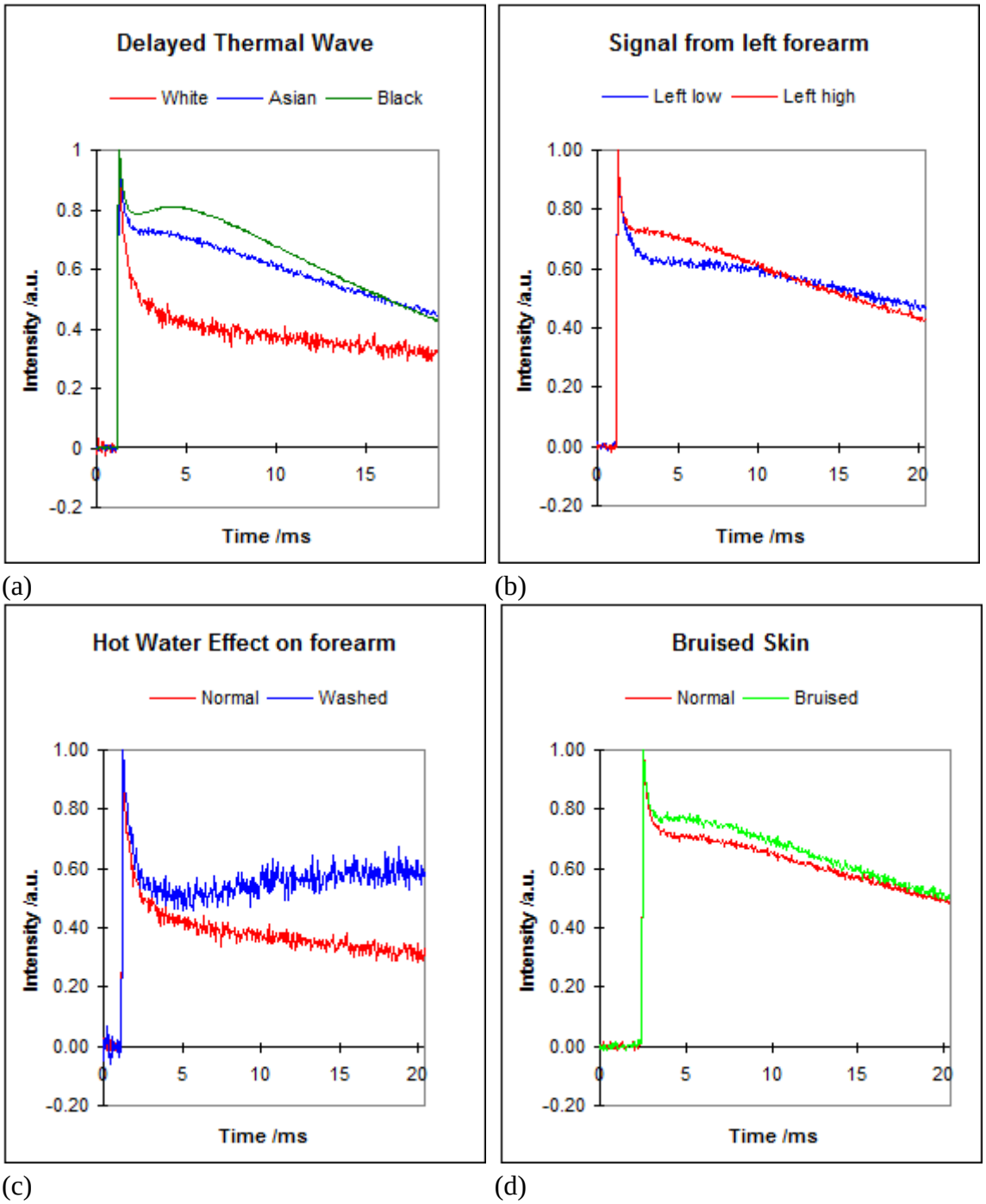

Figure 3. The OTTER signals of different types of skin (a), different position on forearm (b), hot water effect (c), and bruised skin (d) [10].

Figure 3(a) shows the signals from different types of skin, changes in signals are due to melanin differences. Figure 3(b) shows the signals from different positions of the volar forearm, changes in signals are due to epidermis thicknesses changes. Figure 3(c) shows the signals before and after

forearm was washed by hot water, changes in signals are due to haemoglogbin changes, i.e. blood flows to surface. Figure 3(d) shows the signals of normal skin and bruised skin (sport injury, caused by a bump, where blood leaks into tissues under the skin and causes the black-and-blue colour), again, changes in signals are due to blood flowing to skin surface. By fitting the Figure 3 signals using Eq.(5) we can get information about the mean melanin and haemoglobin concentration and mean epidermis thickness. By applying to the inverse analysis techniques, such as singular value decomposition (SVD), Conjugate Gradient (CG) and Maximum Entropy Method (MEM) etc, we can get more information about the skin pigments (melanin and haemoglobin) depth profiles [12,13]. By using different wavelengths with OPO laser, we can also differentiate melanin from haemoglobin [14,15].

3.2. Skin Water Content Measurements

In this case, Er:YAG laser (2.94 μm) is used as the heat source in the measurements, and detection wavelength is 13.1μm. The measurement signal is typically a decay curve. Figure 4 show the typical signals of different skin site (left) and corresponding water concentration depth profiles within skin using SLS fitting technique (right). The results show that forehead, face, and forearm have the highest water content and high gradient. Nail and hair have the lowest water content and low gradient. The curved feature of hair hydration depth profile is likely due to the layered hair structure.

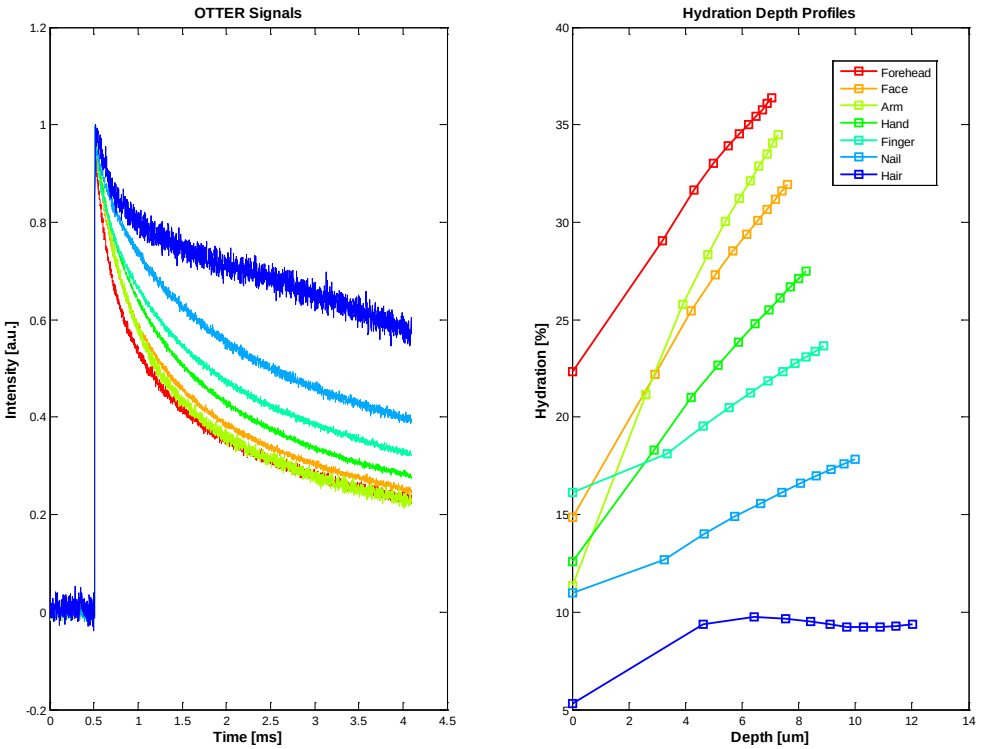

Figure 4. The typical OTTER signals of different skin sites, including hair and nail (left), and the corresponding water concentration depth profiles using SLS fitting technique (right).

By scanning along the surface of volar forearm, we can also produce a 3D water concentration depth profiles within skin, see Figure 5. The result shows that water distribution on the surface is relatively uniform, but the depth profiles are quite different along the arm from wrist to elbow. Across the arm, near the wrist, water distributions are also different from one side to another. This is likely to reflect the stratum corneum thickness changes at different positions of the arm.

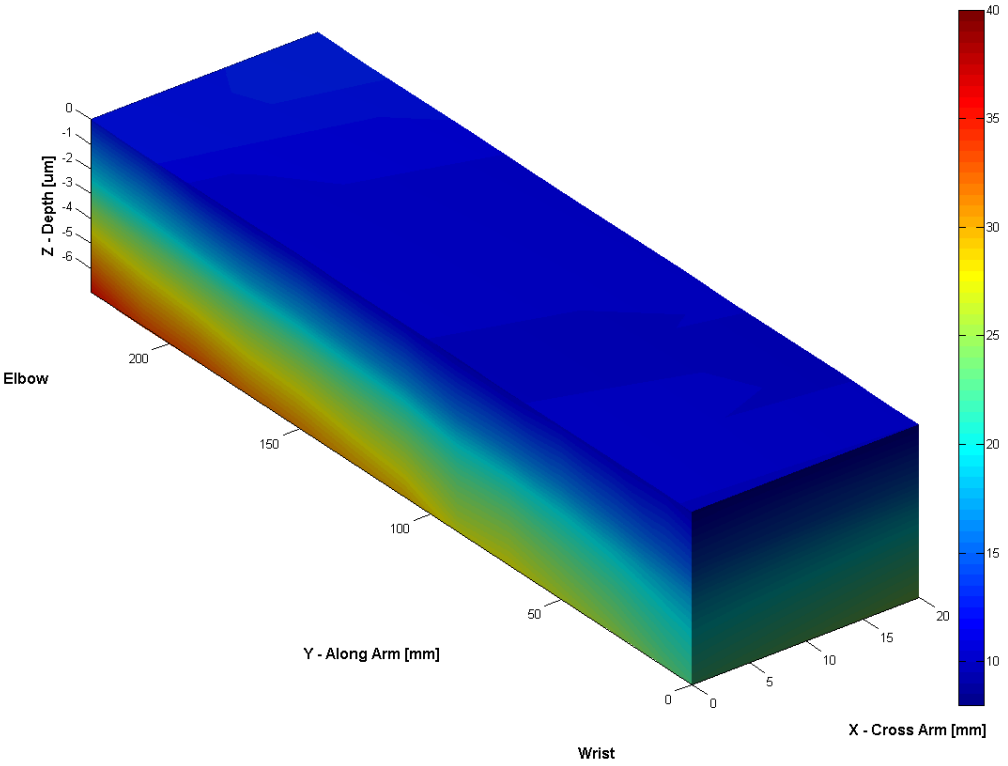

Figure 5. The 3D water concentration depth profiles along the volar forearm.

3.3. Solvent Penetration Measurements

By selecting detection wavelength at 9.5μm, where water has relatively low absorption and chemical solvents have relatively high absorption, we can also measure the solvent penetration through the skin [16, 17, 23, 24]. Figure 6 shows the OTTER results of Dimethyl sulfoxide (DMSO) penetration through skin. In this measurement, a small amount of undiluted DMSO solvent (~ 0.1 ml) is applied on a test skin site for 5 minutes. After the skin surface is wiped dry, tape stripping is performed, in order to see how much and how deep DMSO penetrates. OTTER measurements are performed both before and after the DMSO solvent application, and after each tape stripping, with totally 10 tape strips applied. Figure 6 shows the OTTER signals (left), and the corresponding DMSO concentration depth profiles using SLS fitting technique at different tape stripping (right). The results show a high DMSO concentration immediately after its application, and then as tape stripping continued, deep into the skin, DMSO concentration gradually reduced. Other solvents that have been studied include propylene glycol, ethylene glycol, glycerol, alcohol, decanol, butyl acetate etc [23,24]. OTTER can work well on both in-vivo and in-vitro skin samples.

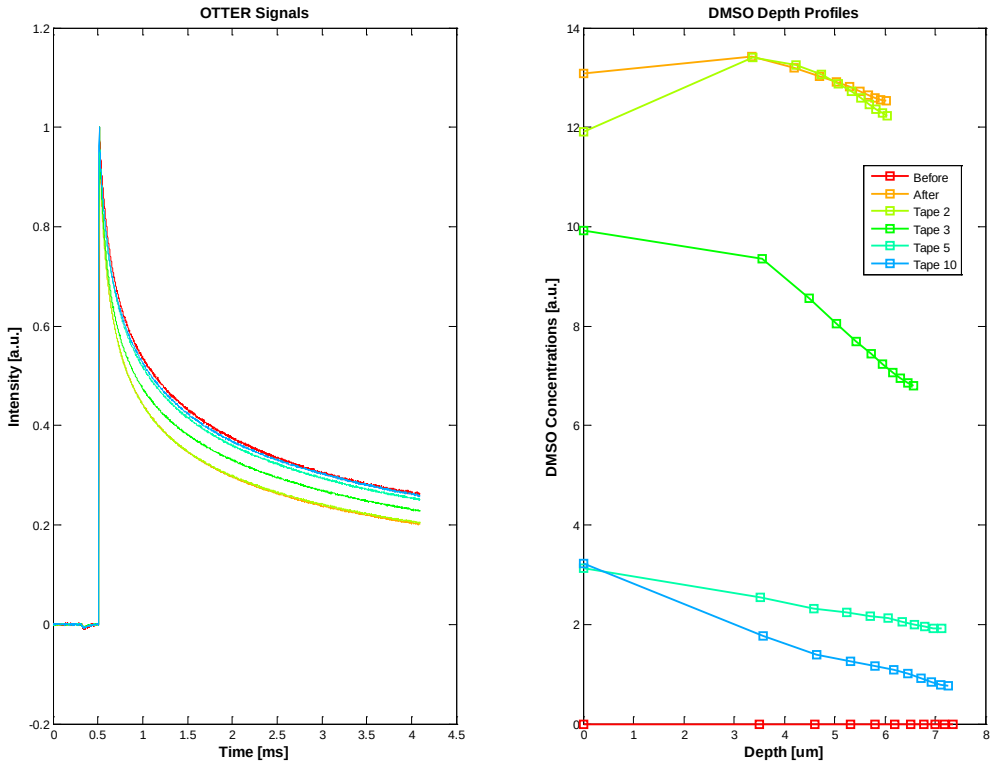

Figure 6. The OTTER signals of DMSO penetrating through skin (left) and the corresponding DMSO concentration depth profiles using SLS fitting technique after different tape stripping (right).

3.4. Nail Measurements

Apart from in-vivo and in-vitro skin samples, OTTER can also work on nails, for both water content measurements and solvent penetration measurements [24,25]. Figure 7 shows the OTTER signals of human fingernail (left) and corresponding water concentration depth profiles before and after a 15 minutes soaking in water (right). In this experiment, a left hand nail was soaked in room temperature water for 15 minutes, then carefully patted dry. The OTTER measurements were performed both before and after soaking. The nail water concentration has increased after the soaking, indicating absorbing of water through soaking, and then as nail recovered in ambient condition, the nail water concentration gradually reduced to the normal level.

Figure 8 shows the solvent penetration through nail measurements, data from [24]. In this experiment, three solvents were studied, glycerol, decanol, butyl acetate. Solvents were applied to the fingernail of a volunteer using a filter pad (Cat. No. 1001 110, Whatman, Kent, U.K.) for a period of 5 min. The pad was then removed, the nail wiped and the solvent decay measured on removal and then at 8 and 10 min after the initial application. Glycerol exhibits the fastest diffusion through nail tissue of the three solvents tested as after 5 min the concentration profile immediately starts to decrease.

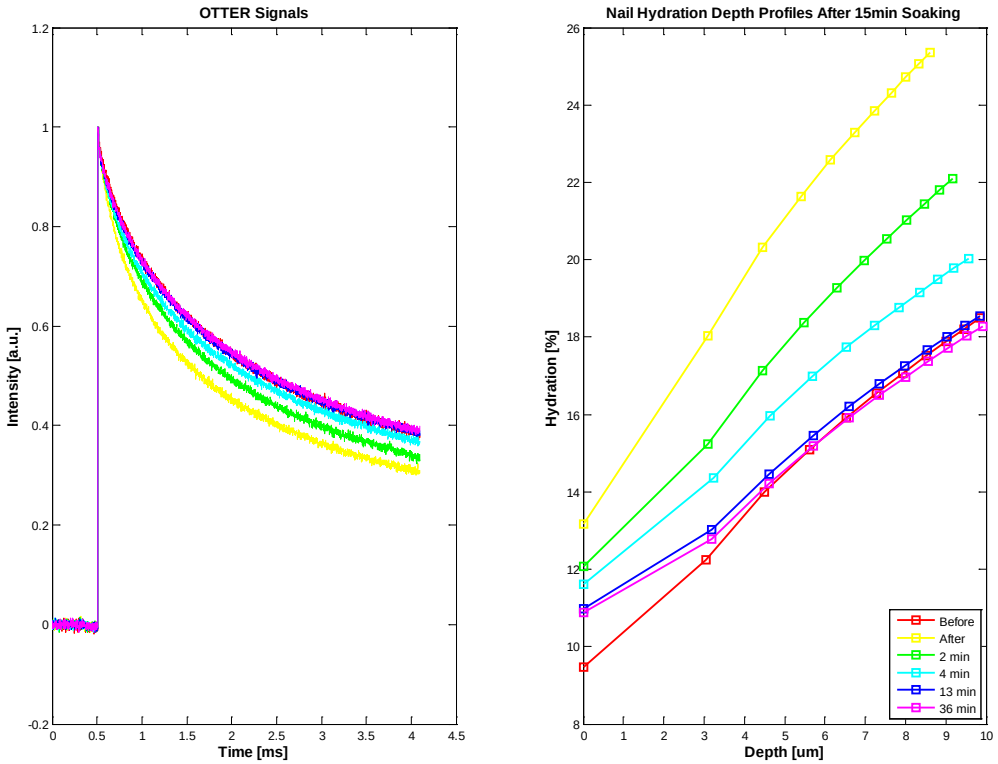

Figure 7. The OTTER signals of in-vivo human fingernail (left) and corresponding water concentration depth profiles using SLS fitting technique before and after a 15 minutes soaking (right).

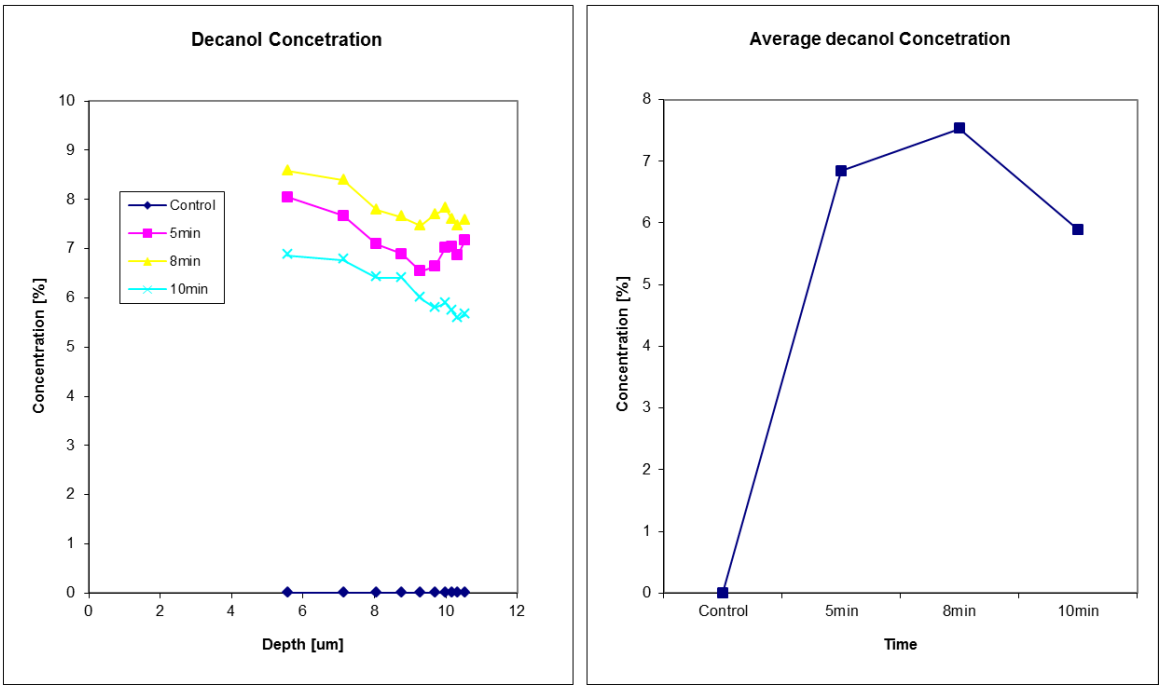

(a)

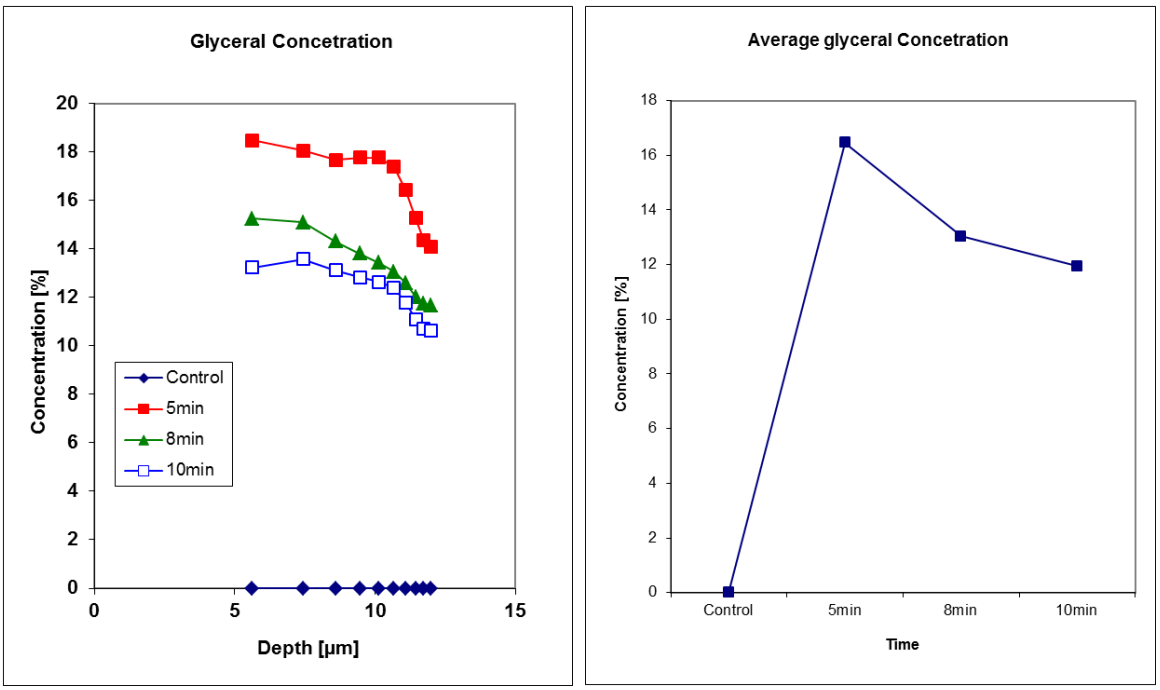

(b)

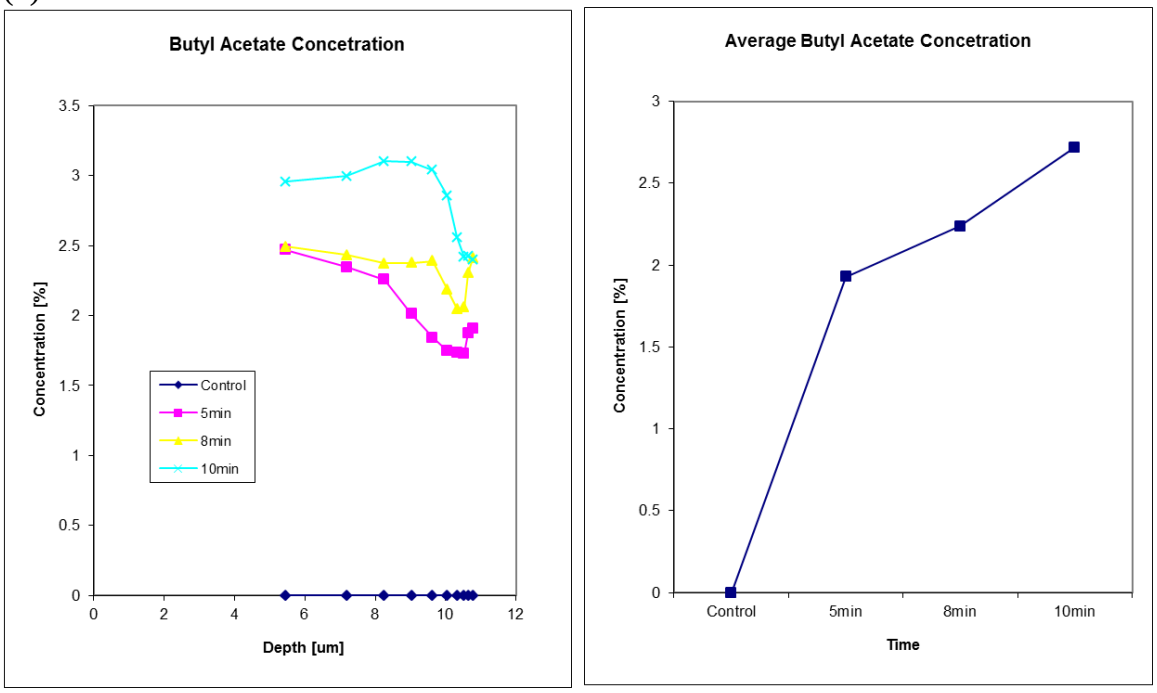

(c)

Figure 8. Solvents depth profiles in in-vivo human fingernail (left), and corresponding relative solvent concentration in nail at 5min, 8min and 10min after the time of solvent application (right), data from [24].

3.5. Hair Measurements

Our latest study shows that OTTER can also be used for hair measurements, despite of low water content in the hair. Figure 9 shows the hair water content measurements. In this experiment, an ex-vivo hair sample, freshly cut from a healthy volunteer, was hydrated by soaking in room temperature for 15

minutes, then patted dry afterwards. The OTTER measurements were performed both before and periodically after the soaking. As explained earlier in Figure 4, the curved feature of hair hydration depth profile is likely due to the layered hair structure. It is interesting to point out that immediately after soaking, this curved feature seems to be disappeared, which might suggest excess water absorbed during soaking has gone into different layers in hair. It is also interesting to point out that it takes more 40 minutes for hair to recovery to its normal hydration level, this is more slower than the skin and the nail in our previous studies [10, 26]. Also, as hair gradually loses its excess water to ambient, the curved feature of hair hydration depth profile started to re-appear back.

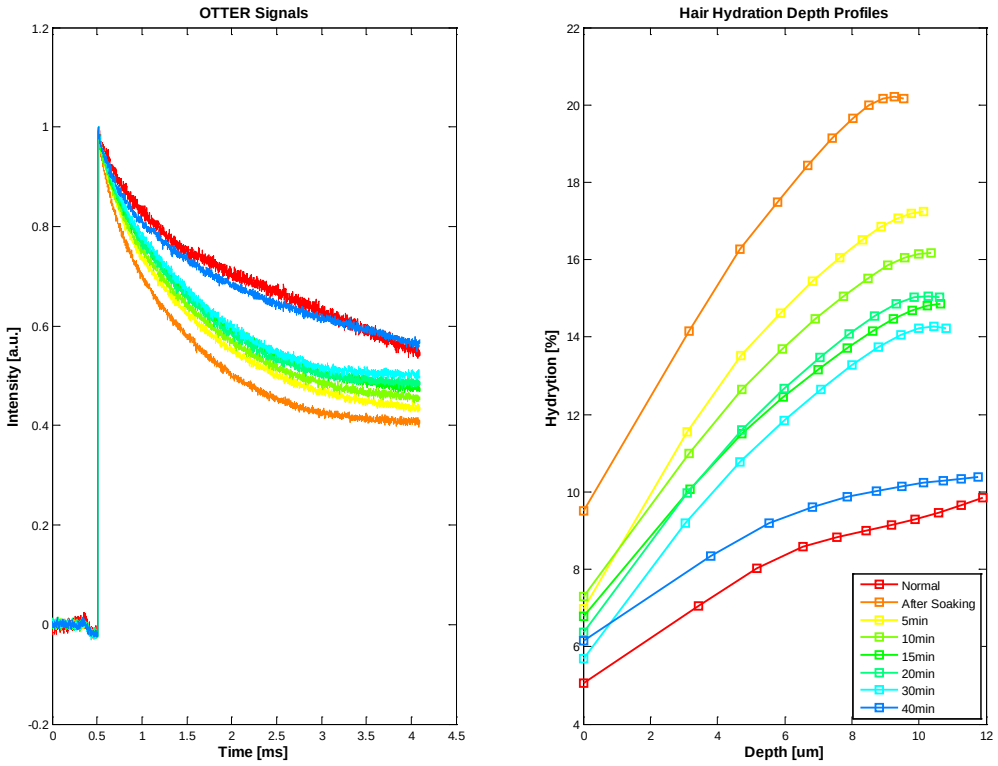

Figure 9. OTTER signals of ex-vivo human hair (left), and corresponding water concentration depth profiles in hair before and after soaking (right).

3.6. Future Developments

By combining photothermal radiometry and FTIR (Fourier Transform InfraRed spectroscopy) [9, 26,27] or diffraction grating [28], it is possible to achieve photothermal spectroscopy. Different from traditional FTIR, photothermal spectroscopy is depth-resolved, which means we can get the spectra information from both skin surface and at different depth underneath the skin surface. This could be very useful for study skin properties, trans-dermal drug delivery, skin active ingredients. By using 2D matrix mercury cadmium telluride (MCT) detector, or X-Y scanning stage, it is also possible to achieve photothermal microscopy. The combination of depth-resolved photothermal spectroscopy and photothermal microscopy will create a whole new measurement technology - Photothermal Hyperspectral Imaging, that is imaging based, non-contact, non-invasive, depth-resolved, and spectroscopic.

4. Conclusions and Future Works

This paper reviews the photothermal radiometry technology for skin and skin appendages research and reports its latest developments. Our studies show that photothermal radiometry can be used for a range of skin measurements, including skin pigments, skin water content, solvent penetrations etc. It can work on skin, nail and hair, both in-vivo and in-vitro. Comparing with other technologies, Photothermal radiometry is non-contact, non-destructive, and spectroscopic in nature. It is quick to make a measurement (a few seconds). It is colour blind, and can work on any arbitrary sample surfaces. Photothermal radiometry also has a unique depth profiling capability around top 20 μm of skin surface. For future works, our studies show that is possible to create a depth-resolved Photothermal Hyperspectral Imaging, which is capable to generate skin images at different infrared wavelengths and at different skin depth. This opens more potential opportunities such as skin disease detection and skin cancer diagnosis etc.

Acknowledgments

We thank London South Bank University for the finance support of this project. We also like to thank EPSRC, BBSRC, Royal Society, and Unilever Port Sunlight Research for the previous support.

Conflicts of Interest

The authors declare no conflict of interest.

References

1. Tam A.C., Sullivan B., “Remote sensing applications of pulsed photothermal radiometry”, Appl. Phys. Lett., 43, 333-335, 1983.
2. Imhof R.E., Birch D.J.S., Thornley F.R., Gilchrist J.R. and Strivens T.A., “Opto-thermal transient emission radiometry”, J. Phys. E: Sci. Instrum., 17, 521-525, (1984).
3. Long F.H., Anderson R.R., and Deutsch T.F., “Pulsed photothermal radiometry for depth profiling of layered media”, Appl. Phys. Lett., 51, 2076-2078, 1987.
4. Jacques S.L., Nelson J.S., Wright W.H., and Milner T.E., “Pulsed photothermal radiometry of port-wine-stain lesions”, Applied Optics, 32, 2439-2446,1993.
5. Vitkin I.A., Wilson B.C., Anderson R.R., Prahl S.A., “Pulsed photothermal radiometry in optically transparent media containing discrete optical absorbers”, Phy. Med. Biol., 39, 1721-1744, 1994.
6. Almond D.P. and Patel P.M., Photothermal Science and Techniques, ASIN: B017PNMQS8, Chapman and Hall, 1996.
7. Vavilov V.P., Burleigh D.D., Review of pulsed thermal NDT: Physical principles, theory and data processing, NDT & E International, Volume 73, July 2015, Pages 28–52. doi:10.1016/j.ndteint.2015.03.003.
8. Imhof R.E., Zhang B. and Birch D.J.S., “Photothermal Radiometry for NDE”, in Mandelis A (ed): Progress in Photothermal and Photoacoustic Science and Technology. PTR Prentice Hall, Englewood Cliffs (USA), vol. II, pp 185-236, 1994.

9. Imhof R.E., McKendrick A.D. and Xiao P. , "Thermal emission decay Fourier transform infrared spectroscopy", Rev. Sci. Instrum., 66, 5203-5213, 1995.
10. Xiao P. , “Opto-Thermal Mathematical Modeling and Data Analysis in Skin Measurements”, Ph.D. thesis, London South Bank University, 1997.
11. Xiao P. and Imhof R.E. , "Inverse Method Analysis in Opto-Thermal Skin Measurements", SPIE Proc., 3601, pp340-347, 1999.
12. Xiao P., Gull S.F. and Imhof R.E. , “Opto-Thermal Inverse Modelling Using a Maximum Entropy Approach”, Analytical Sciences, Vol 17 Special Issue, pp s394- s397, 2001.
13. Xiao P. , Guo X., Notingher I., Cowen J.A., O'Driscoll D. and Imhof R.E. , "Opto- Thermal Skin Pigment Spectral Depth Profiling using an OPO Laser", SPIE Proc., 3601, pp348-354, 1999.
14. Xiao P., Cowen J.A., Guo X., O'Driscoll D. and Imhof R.E. , "Photothermal In-vivo Characterization of Human Skin using Tuneable OPO laser Excitation", Photoacoustic and Photothermal Phenomena: 10the International Conference, edited by F. Scudieri and M. Bertolotti, 621-623, 1999.
15. Xiao P. and Imhof R.E. , "Opto-thermal measurement of water distribution within the stratum corneum", Skin Bioengineering Techniques and Applications in Dermatology and Cosmetology, Curr Probl Dermatol, Basel: Karger, 26, 48-60, 1998.
16. Xiao P., Cowen J.A. and Imhof R.E., “In-Vivo Transdermal Drug Diffusion Depth Profiling - A New Approach to Opto-Thermal Signal Analysis”, Analytical Sciences, Vol 17 Special Issue, pp s349-s352, 2001.
17. Xiao P., Ou X., Ciortea L.I., Berg E.P.,· Imhof R.E., "In Vivo Skin Solvent Penetration Measurements Using Opto-thermal Radiometry and Fingerprint Sensor", Int J Thermophys (2012) 33:1787–1794. DOI 10.1007/s10765-012-1318-6.
18. Xiao P. and Imhof R.E. , “Data Analysis Technique for Pulsed Opto-Thermal Measurements”, UK Patent Application 0004374.5, 2000.
19. Xiao P. and Imhof R.E. , “Apparatus for in-vivo Skin Characterization”, UK Patent Application GB1014212.3, 2010.
20. Scheuplein R.J., “A survey of some fundamental aspects of the absorption and reflection of light by tissue”. J Soc Cosmet Chem, 15:111-122, 1964.
21. Jacques S.L., “Laser Tissue Interactions”. Lasers in General Surgery, 72, 531-557, 1992.
22. Yoon G., Welch A.J., Motamedi M., Van Gement M.C.J., “Development and application of Three-Dimentional Light Distribution Model for Laser Irradiated Tissue”. IEEE J. Quan. Elec. Vol QE-23, no. 10, 1987.
23. Cowen J.A., In-vivo Opto-thermal Transdermal Diffusion Measurement, PhD thesis, London South Bank University, 1999.
24. Xiao P., Zheng X., Imhof R.E., Hirata K., McAuley W.J., Mateus R., Hadgraft J., Lane M.E., “Opto-Thermal Transient Emission Radiometry (OTTER) to image diffusion in nails in vivo ”, International Journal of Pharmaceutics 406 (2011) 111– 113.
25. Xiao P., Ciortea L.I., Singh H., Berg E.P. and Imhof R.E. , "Opto-thermal Radiometry for In-Vivo Nail Measurements", Journal of Physics: Conference Series vol. 214, no 1, 012008, 2009.

371 26. Notingher I., Imhof R.E. , Xiao P., Pascut F.C., “Spectral Depth Profiling of Arbitrary Surfaces by
372 Thermal Emission Decay-Fourier Transform Infrared Spectroscopy”, Applied Spectroscopy, Vol
373 57, No. 12, pp1494-1501, 2003.
374 27. Notingher I., Imhof R.E., Xiao P., Pascut F.C., “Near-surface depth-resolved midinfrared
375 emission spectroscopy”, *Rev. Sci. Instrum*., Vol 74, No. 1, pp 346 - 348, 2003.
376 28. Pascut F.C., Fiber-Optic Optothermal Emission Radiometry for In-vivo Skin Measurements, PhD
377 thesis, London South Bank University, 2004.